scientific reports

Check for updates

OPEN

Stochastic resonance analysis of a coupled high-speed maglev vehicle-bridge coupled system under bounded noise

Yan-xia Li[1,2]✉, Zhi-wu Yu[1,2] & Lei Xu[1,2]

Coupled oscillations typically occur in maglev vehicle-bridge coupled systems excited by bounded noise caused by guideway irregularities. The paper employed Hamilton equations to derive the corresponding canonical transformation equations and determined the critical stable regions for two kinds of resonances using the largest Lyapunov exponents. The results show that the critical stable region between the excitation amplitude and the resonant frequency ratio is a valley shape when the system has external resonance only. When considering both internal and external resonances, the critical stable region between the excitation amplitude and resonant frequency ratio presents a small saddle shape. Energy transfers from the first to the second oscillator under with both internal and extrinsic resonance. As the guideway irregularities' coefficients increase, the maximum Lyapunov exponents of the two conditions change from negative to positive, which means that the system varies from a stable state to instability.

Electromagnetic suspension (EMS) system[1] is becoming increasingly popular in urban transportation due to its high speed. Compared with wheel/rail trains which are typically propelled by motors and adhesive forces, maglev vehicles are suspended in the air through electromagnetic induction [2–5] and are more sensitive to internal excitation, external excitation, air gap floating, circuit fluctuations, and bridge vibrations. Therefore, suppression methods for resonances have encountered various challenges such as moving loads, dynamic deflection, heterogeneous frequencies, invalid controllers, faulty suspension magnets, bridge's lightweight, and unmatched indices [6].

The test results of the Shanghai maglev line and the German EMSLAND line show that the dynamic loads' factor of the two-span track beam is less than 1.2 and the local dynamic loads' factor is less than 1.5 over the whole speed range. To prevent the vehicle-bridge coupled system's resonance, the DIN (Deutsche Industrie Norm) standards stipulate that the product of the beam's fundamental frequency and a single hole span need to be equal to 1.1 times the speed limit. It has been observed that the natural frequencies of the suspension system and the track are equal to 4.8 Hz and 17 Hz, respectively. However, because the track has a large oscillation amplitude[7], the resonance needs to be calculated based on thorough analyses.

In this paper, a series of approaches for calculating resonance were presented including the average power for moving distribution loads' method and the Lyapunov method. The average power technique was based on the transfer function and the stable condition described by Li Jinhui[8–10], who provided the minimum model of the maglev vehicle-bridge interaction system, the necessary conditions for its stability, and three principles underlying the self-excited vibration. The resonant conditions under moving distribution loads were improved by Fryba, Yau J. D., Kwark, Xia H., and Yang Y. B.[11–15], who gave the critical speeds at which the resonance may occur, thought the maximum acceleration responses of the beam to be dominated by the fundamental vibration modals, presented the numerical method technique concerning the dynamic behavior of bridges, explained the mechanisms of resonances and cancellation, and proposed the resonant formulas for calculating the span and frequency. The effect of fuzzy controller was discussed by Sun Yougang[16], which can improve the dynamic performance of the system, make the maglev system obtain a large stable range, and restrain the vehicle–guideway interaction vibration effectively.

Noise is commonly considered undesirable. However, some special nonlinear systems have nonintuitive dynamic behaviors after noise is introduced. Indeed, in recent years, there have been several studies to demonstrate the phenomenon of stochastic resonance (SR). Examples were: (i) an experiment demonstrating stochastic

[1]Central South University, Changsha 410075, China. [2]National Engineering Center of High-Speed Railway Construction, Changsha 410075, China. ✉email: 3132154012@qq.com

resonance in a bistable electronic device: a tunnel diode [17]. Stochastic resonance was detected using a simple experimental setup by investigating the time evolution of the voltage measured across the tunnel diode as a function of the input noise intensity. (ii) the stochastic resonant phenomena was studied experimentally and theoretically for a state-of-the-art metal-oxide memristive device based on yttria-stabilized zirconium dioxide and tantalum pent-oxide, which has exhibited bipolar filamentary resistive switching of the anionic type [18]. The optimal noise intensity corresponding to the stochastic resonance phenomenon was interpreted using a stochastic memristor model by adding an external noise source to the control voltage. Furthermore, dynamical systems have been studied in the presence of relevant noise-induced phenomena with a constructive role in stability, such as, (i) the damping-enhanced stability of a Brownian particle starting from an unstable initial position and moving in a metastable system was explored [19]; (ii) a memristor used for resistive switches behaved as multistable nonlinear systems between low-resistance and high-resistance states in a random telegraphic signal mode [20]; (iii) an approach using a real stable polynomial combined with a Gauge transformation was presented and the bistability of polynomials corresponding to factors of the original multi-graph model resulted in real stable polynomials of each factor in various multi-graph models of the aforementioned contraction sequence [21]; (iv) a nonstationary function within a memristive system was investigated to devise a simplified description of transient processes under different noise intensities, and the relaxation time was obtained, which depended nonmonotonically on the intensity of the fluctuations [22]. Finally, in other scientific study fields, such as quantum phase transitions in complex biological and physical systems, the positive role of noise has also been demonstrated. For example: (i) the Gaussian non equilibrium steady states of the quantum characteristics of such critical phenomena have been reviewed [23]. (ii) a quantum case has been detected in which the indeterminacy arising from the uncertainty principle reduced the accuracy of the parameter estimation in a way that cannot be neglected, even in the limit of infinite copies[24]. (iii) the phenomena of dissonance and consonance have considered, where two sensory neurons were driven by noise and subthreshold periodic signals, and their outputs plus noise were applied to a third neuron with noise added to them [25]; (iv) the noise in the high resistive state was found to be featured by nearly the same probability density functions and spectrum as the inner noise of the experimental setup [26].

Compared with previous research frameworks of time-domain samples in Newtonian mechanics, a Hamiltonian system with narrow-band random excitation is more complex. Some theoretical bases have been proposed. Colored noise refers to a fixed centre frequency, white noise intensity, and a uniform distribution angle with a triangular relationship [27,28], which examined the responses. This noise was utilized in a Wiener process by an equivalent to measured power spectra in methods put forward by Chen Zeshen, Jin Zhibin, and Jin Shi [29–31], who performed the theoretical modeling analysis in the time domain with covariance analysis method, generated guideway irregularities by combining the shape filter with the time delay system, and considered short-wavelength track irregularities. Some examples substantiated in bridge responses under wind loads have been obtained by Dimentberg M, Lin Y.K., and Jian Deng. [32–34], who obtained the subcritical responses to an external broadband random, considered turbulence stabilize even a single-degree of freedom structural motion, and provided insights on how to analyze and control parametric resonances under a bounded noise process in engineering applications. Since Lyon et al. first applied a stochastic averaging method[35] proposed by R. L. Stratonovich[36], it was subsequently applied by Zhu W. Q., Huang Z. L., Liu Zhonghua, and W.Y. Liu[37,38], who proposed a stochastic averaging method to predict approximately the response of quasi-integrable Hamiltonian systems excited by bounded noise, determined the threshold of bounded noise amplitude for the onset of chaos. They have applied to duffer oscillator analyses using the random mean principle and the limited differential technique. Although Bo Zhang[39] investigated the random stability of a suspended wheelset system considering Gaussian white noise by the random average method. At present, there are few studies on resonance based on stochastic stability. Solving the resonant behaviour of the complex maglev vehicle-bridge coupled system is key to the further development of EMS.

The study presented in this paper aims to build a model to explore the critical conditions of stochastic resonance over the whole bridge span with the aerodynamic loads and guideway irregularities. Hamilton's theory is applied to derive the differential equations and their dimensionless equations [28]. The appropriate stable domains at different resonances based on stochastic averaging theory and canonical transformations are given. The stability probability according to the Fokker–Planck–Kolmogorov (FPK) equation utilized in this study. Moreover, a unique numerical method for assessing the effects of aerodynamic loads and the guideway excitation on the stochastic resonance of the maglev vehicle-bridge coupled system is also presented.

The stochastic averaging method

To explain the theoretical basis of our model's analysis, the derivation process of the stochastic averaging method is introduced below.

Consider a quasi-integrable Hamiltonian system under bounded noise excitation governed by the following equations of motion[37]:

$$\dot{Q}_i = \frac{\partial H}{\partial P_i}\ \dot{P}_i = -\frac{\partial H}{\partial Q_i} - \varepsilon c_{ij}\frac{\partial H}{\partial P_i} + \varepsilon h_{ij}\xi_k(t)\ \ i,j = 1,...,n;\ k = 1,...,l \tag{1}$$

where Q_i and P_i are the generalized displacements and momentum, respectively; $H = H(Q, P)$ is the Hamiltonian; $\varepsilon c_{ij} = \varepsilon c_{ij}(Q, P)$ are the coefficients of lightly linear or nonlinear damping; $\varepsilon h_{ij} = \varepsilon h_{ij}(Q, P)$ denotes the amplitudes of weak bounded noises; and $\xi_k(t)$ represents independent bounded noises of the form

$$\xi_k(t) = cos[\Omega_k t + \sigma_k B_k(t) + \Delta_k]\ \ k = 1,...,l \tag{2}$$

where Ω_k and σ_k^2 are constants representing the center frequencies and strengths of the frequency perturbations, respectively; $B_k(t)$ are independent units in the Wiener processes; and Δ_k are independent random phases that

are uniformly distributed in $[0, 2\pi]$. $\xi_k(t)$are independent stationary random processes in a wide sense with spectral densities

$$S_k(\omega) = \frac{\sigma_k^2}{4\pi} \frac{\sigma_k^2 + \omega^2 + \sigma_k^4/4}{(\omega^2 - \Omega_k^2 - \sigma_k^4/4) + \sigma_k^4\omega^2} \tag{3}$$

and auto correlation functions

$$R_k(\tau) = \frac{1}{2} exp(-\frac{\sigma_k^2}{2}|\tau|) cos\Omega_k\tau \tag{4}$$

The bandwidths of the processes $\xi_k(t)$ depend mainly on the parameters σ_k. The processes are narrow-banded when σ_k are small and wide-banded processes when σ_k are large. It is assumed that σ_k are small and thus the corresponding processes are narrow-band.

Suppose that the Hamiltonian system shown with Eq. (1) with $\varepsilon = 0$ is integrable, i.e., there exists a set of canonical transformations

$$I_i = I_i(Q, P), \theta_i = \theta_i(Q, P)\ i = 1, ..., n \tag{5}$$

through which new Hamiltonian equations are of the following form:

$$\dot{\theta}_i = \frac{\partial H(I)}{\partial I_i} = \omega_i(I)\ \dot{I}_i = -\frac{\partial H(I)}{\partial \theta_i} = 0\ i = 1, ..., n \tag{6}$$

where I_i and ω_i are action variables and frequencies, respectively; θ_i are the angle variables conjugated to I_i; and $H(I)$ is the transformed Hamiltonian, which is independent of θ_i. The Hamiltonian system is resonant if there exist $\alpha(1 \le \alpha \le n-1)$ resonant relations such that

$$L_i^u\omega_i = 0\ u = 1, ..., \alpha \tag{7}$$

where L_i^u are integers that are not all zero for a fixed u.

By using the canonical transformations of Eq. (5), the differential equations for the action and angle variables of the quasi-integrable Hamiltonian system (1) can be obtained from Eq. (1) as follows:

$$\begin{aligned} \dot{I}_r &= \varepsilon\left(-c_{ij}\frac{\partial H}{\partial P_j}\frac{\partial I_r}{\partial p_i} + h_{ik}\xi_k(t)\frac{\partial I_r}{\partial P_i}\right) \\ \dot{\theta}_r &= \omega_r - \varepsilon c_{ij}\frac{\partial H}{\partial P_j}\frac{\partial \theta_r}{\partial p_i} + \varepsilon h_{ik}\xi_k(t)\frac{\partial \theta_r}{\partial P_i} \\ r, i, j &= 1, ..., n;\ k = 1, ..., l \end{aligned} \tag{8}$$

The form and dimension of the averaging equations depend on the resonance of the Hamiltonian system described in Eq. (8). In the following subsections, two cases are considered.

External resonance only. Consider a system with external resonance but no internal resonance. Suppose that there are β external primary resonant relations between the first β oscillators and the first β bounded excitations, i.e.,[27]

$$M_\nu\Omega_\nu + L_\nu\omega_\nu = \varepsilon\delta_\nu\ \upsilon = 1, ..., \beta \tag{9}$$

where M_ν and L_ν are positive or negative integers and there is no summation over subscript υ. Introduce β new variables:

$$\psi_\nu = M_\nu(\Omega_\nu t + \sigma_\nu B_\nu(t) + \Delta_\nu) + L_\nu\theta_\nu \tag{10}$$

Using the transformation in Eq. (10), the differential equations for $I_1, ..., I_n, \psi_1 ...., \psi_n, \theta_1 ...., \theta_n$ can be obtained from Eq. (8) as follows:

$$\begin{aligned} \frac{dI_r}{dt} &= \varepsilon\left[-c_{ij}\frac{\partial H}{\partial p_j}\frac{\partial I_r}{\partial p_i} + h_{ik1}\frac{\partial I_r}{\partial p_i}cos\left(\frac{1}{M_{k1}}\psi_{k1} - \frac{L_{k1}}{M_{k1}}\theta_{k1}\right) + h_{ik2}\frac{\partial I_r}{\partial p_i}\xi_{k2}(t)\right] \\ &= \varepsilon U_r(I, \psi, \theta) + \varepsilon h_{ik2}\frac{\partial I_r}{\partial p_i}\xi_{k2}(t) \\ \frac{d\psi_\nu}{dt} &= \varepsilon\left[\delta_\nu - L_\nu c_{ij}\frac{\partial H}{\partial p_j}\frac{\partial \theta_\nu}{\partial p_i} + L_\nu h_{ik1}\frac{\partial \theta_\nu}{\partial p_i}cos(\frac{1}{M_{k1}}\psi_{k1} - \frac{L_{k1}}{M_{k1}}\theta_{k1}) + L_\nu h_{ik2}\frac{\partial \theta_r}{\partial p_i}\xi_{k2}(t)\right] \end{aligned}$$

$$+M_\nu\sigma_\nu\frac{dB_V(t)}{dt}$$

$$=\varepsilon V_r(I,\psi,\theta)+\varepsilon L_\nu h_{ik2}\frac{\partial\theta_\nu}{\partial p_i}\xi_{k2}(t)+M_\nu\sigma_\nu\frac{dB_\nu(t)}{dt}$$

$$\frac{d\theta_r}{dt}=\omega_r-\varepsilon c_{ij}\frac{\partial H}{\partial p_j}\frac{\partial\theta_r}{\partial p_i}+\varepsilon h_{ik1}\xi_k(t)\frac{\partial\theta_r}{\partial p_i})$$

$$r,i,j=1,...,n;\ k_1,\nu=1,...,\beta;\ k_2=\beta+1,...,l;\ k=1,...,l \tag{11}$$

where $I=(I_1,...,I_n),\psi=(\psi_1,...,\psi_\beta),\theta=(\theta_1,...,\theta_n)$

As shown in Eq. (11), $I_1,...,I_n$, and $\psi_1,...,\psi_\beta$ are slowly-varying processes, while $\theta_1,...,\theta_n$ are rapidly varying processes. By applying deterministic averaging to $\theta_1,\ldots,\theta_n$, the averaged $IT\dot{O}$ equations can be defined as follows:

$$\mathrm{d}I_r=\varepsilon\widetilde{U}_r(I,\psi)dt\mathrm{d}\psi_\nu=\varepsilon\widetilde{V}_r(I,\psi)dt+M_\nu\sigma_\nu dB_\nu(t)$$

$$r=1,...,n;\ \nu=1,...,\beta \tag{12}$$

where

$$\widetilde{U}_r=\frac{1}{(2\pi)^n}\int_0^{2\pi}U_r(I,\psi,\theta)\ \ d\theta\,\widetilde{V}_r=\frac{1}{(2\pi)^n}\int_0^{2\pi}V_r(I,\psi,\theta)d\theta \tag{13}$$

The averaged FPK equation associated with Eq. (12) is

$$\frac{\partial p}{\partial t}=-\varepsilon\frac{\partial(\widetilde{U}_r p)}{\partial I_r}-\varepsilon\frac{\partial(\widetilde{V}_r p)}{\partial\psi_\nu}+\frac{M_\nu^2\sigma_\nu^2}{2}\frac{\partial^2 p}{\partial\psi_\nu^2} \tag{14}$$

where $p=p(I,\Psi,0|I_0,\psi_0)$ is the transition probability density. The initial condition of Eq. (14) is

$$p=p(I,\Psi,0|I_0,\psi_0)=\delta(I-I_0)\delta|(\psi-\psi_0) \tag{15}$$

The boundary conditions with respect to ψ_ν are periodic, i.e.,

$$p|_{\Psi_n+2n\pi}=p|_{\psi_n})\quad\frac{\partial p}{\partial\psi_\nu}|_{\Psi_n+2n\pi}=\frac{\partial p}{\partial\psi_\nu}|_{\psi_n} \tag{16}$$

$$u,\nu=1,...,\beta$$

The boundary conditions with respect to I_r are defined as

$$p=finite\ at\ I_r=0 \tag{17}$$

$$p,\frac{\partial p}{\partial I_r}\to 0\,as\ I_r\to\infty \tag{18}$$

The reduced FPK equation with its boundary conditions can be solved numerically by using the combination of finite difference method and the successive over-relaxation method.

Both internal and external resonance. Consider a system with β external resonant relations and α internal resonant relations, i.e.,

$$M_\nu\Omega_\nu+L_\nu\omega_\nu=\varepsilon\delta_\nu\quad\sum_{i=1}^{n}N_i^u\omega_i=\varepsilon\sigma_u\ \upsilon=1,...,\beta;\ \ u=1,...,\alpha \tag{19}$$

where M_ν and L_ν are positive or negative integers and there is no summation over subscript ν. The N_i^u are also integers that are not all zero for a given u. Then new variables are introduced[37]:

$$\psi_\nu=M_\nu(\Omega_\nu t+\sigma_\nu B_\nu(t)+\Delta_\nu)+L_\nu\theta_\nu$$

$$\Phi_u=\sum\nolimits_{i=1}^{n}N_i^u\theta_i\ \ \nu=1,\ldots,\alpha \tag{20}$$

The transformation is shown in Eq. (20), the differential equations for I,ψ,Φ, and θ_1 can be obtained from Eq. (8) as follows.

$$\frac{dI_r}{dt} = \varepsilon\left[-c_{ij}\frac{\partial H}{\partial p_j}\frac{\partial I_r}{\partial p_i} + h_{ik1}\frac{\partial I_r}{\partial p_i}cos(\frac{1}{M_{k1}}\psi_{k1} - \frac{L_{k1}}{M_{k1}}\theta_{k1}) + h_{ik2}\frac{\partial I_r}{\partial p_i}\xi_{k2}(t)\right]$$

$$= \varepsilon U^{'}{}_r(I,\psi,\Phi,\theta_1) + \varepsilon h_{ik2}\frac{\partial I_r}{\partial p_i}\xi_{k2}(t)$$

$$\frac{d\psi_v}{dt} = \varepsilon\left[\delta_v - L_v c_{ij}\frac{\partial H}{\partial p_j}\frac{\partial \theta_v}{\partial p_i} + L_v h_{ik1}\frac{\partial \theta_v}{\partial p_i}cos(\frac{1}{M_{k1}}\psi_{k1} - \frac{L_{k1}}{M_{k1}}\theta_{k1}) + L_v h_{ik2}\frac{\partial \theta_r}{\partial p_i}\xi_{k2}(t)\right]$$

$$+M_v\sigma_v\frac{dB_V(t)}{dt}$$

$$= \varepsilon V^{'}{}_r(I,\psi,\Phi,\theta_1) + \varepsilon L_v h_{ik2}\frac{\partial \theta_v}{\partial p_i}\xi_{k2}(t) + M_v\sigma_v\frac{dB_v(t)}{dt}$$

$$\frac{d\Phi_u}{dt} = \varepsilon\left(\sigma_u - N^u_{u_1}c_{ij}\frac{\partial H}{\partial p_j}\frac{\partial \theta_{u_1}}{\partial p_i} + N^u_{u_1}h_{ik1}\frac{\partial \theta_{u_1}}{\partial p_i}\right) \times cos\left(\frac{1}{M_{k1}}\psi_{k1} - \frac{L_{k1}}{M_{k1}}\theta_{k1}\right)$$
$$+ N^u_{u_1}h_{ik2}\frac{\partial \theta_{u_1}}{\partial p_i}\xi_{k_2} = \varepsilon W^{'}{}_u(I,\psi,\Phi,\theta_1) + \varepsilon N^u_{u_1}h_{ik2}\frac{\partial \theta_{u1}}{\partial p_i}\xi_{k2}(t)$$

$$\frac{d\theta_s}{dt} = \omega_s - \varepsilon c_{ij}\frac{\partial H}{\partial p_j}\frac{\partial \theta_s}{\partial p_i} + \varepsilon h_{ik}\xi_k(t)\frac{\partial \theta_s}{\partial p_i}$$

$$r,i,j,u = 1,...,n;\ k_1,v = 1,...,\beta;\ u = 1,...,\alpha;\ k_2 = \beta+1,...,l;\ k = 1,...,l;\ s = \alpha+1,...,n \tag{21}$$

where $I = (I_1,...,I_n)$, $\psi = (\psi_1,...,\psi_\beta)$, $\Phi = (\Psi_1,\ldots,\Psi_\alpha)$, $\theta_1 = (\theta_\alpha,...,\theta_n)$ and $\theta_1,...,\theta_n$ are replaced by $\Psi_1,...,\Psi_\alpha,\theta_{\alpha+1},...,\theta_n$.

In Eq. (21), I, ψ, and Φ are slowly varying processes, while θ_1 is a rapidly varying process. By applying deterministic averaging to θ_1 to Eq. (21), the averaging $IT\widehat{O}$ equations for I, ψ, and Φ can be expressed as:

$$\mathrm{d}I_r = \varepsilon\widetilde{U}_r(I,\psi,\Phi)dt$$

$$\mathrm{d}\psi_v = \varepsilon\widetilde{V}_r(I,\psi,\Phi)dt + M_v\sigma_v dB_v(t)$$

$$\mathrm{d}\Phi_u = \varepsilon\widetilde{W}_u(I,\psi,\Phi)dt \tag{22}$$

$$\widetilde{U}_r = \frac{1}{(2\pi)^{n-\alpha}}\int_0^{2\pi} U^{'}{}_r(I,\psi,\Phi,\theta_1)d\theta_1 \qquad \widetilde{V}_v = \frac{1}{(2\pi)^{n-\alpha}}\int_0^{2\pi} V^{'}{}_v(I,\psi,\Phi,\theta_1)d\theta_1$$

$$\widetilde{W}_u = \frac{1}{(2\pi)^{n-\alpha}}\int_0^{2\pi} W^{'}{}_u(I,\psi,\Phi,\theta_1)d\theta_1 \tag{23}$$

The averaging FPK equation associated with Eq. (22) is of the form

$$\frac{\partial p}{\partial t} = -\varepsilon\frac{\partial \widetilde{U}_r P}{\partial I_r} - \varepsilon\frac{\partial(\widetilde{V}_r P)}{\partial \psi_r} - \varepsilon\frac{\partial(\widetilde{W}_u P)}{\partial \Phi_u} + \frac{M_v^2\sigma_v^2}{2}\frac{\partial^2_p}{\partial \psi_v^2} \tag{24}$$

Reduced averaged FPK equation (24) under similar boundary conditions can be solved numerically by using a finite difference method and the successive over-relaxation method.

Motion model

To better introduce the case applications, we first provide a detailed description of the composition of the specific model and the parameter settings is provided.

Theoretical hypothesis. In general, model complexity is determined according to the purpose of the model. The model should be sufficiently comprehensive to allow the reliable and accurate analysis of vibration response analyses in terms of ride comfort and safety. Motion stability of an EMS model refers to the parameters for a minimal coupling model composed of a maglev vehicle and a bridge including the elite segments proposed by Jin-hui Li [6]. Depending on the basic elements analyzed, the complex systems is then simplified to minimum models, which is more efficient. Table 1 lists the correlation variables.

The fundamental assumptions are described as follows:

- Electromagnet forces are linear.
- The system is decoupled both laterally and vertically without considering the turning radius, height difference or rolling freedom.
- The random irregularity is bounded noise applied with the shaping filter technique.
- A Bernoulli–Euler beam is adopted for the calculation of the bridge model.
- The moving mass and the action point of the concentrated force are at the geometric center of the electromagnets.

Modelling of substructures. *Bridge model.* Based on the above analysis, the minimal model is presented in Fig. 1 [6,10,40]. The loads of vehicle and passengers are equivalent to a weight force acting on the center of the electromagnetic mass. The vehicle-bridge coupled system can be described using the structure is shown in Fig. 1. The electromagnetic forces are uniformly distributed on the bridge and the electromagnet. The current or voltage of the magnet that controls the electromagnetic action is applied to adjust the gap between the electromagnet and the bridge. The bridge is also shown in Fig. 1, where the endpoint marked with "0" is taken as the coordinate origin. The direction of the hammer is the positive direction of y-axis. Considering the high stiffness of the electromagnet, its deformation in the y-direction can be ignored. The dynamic characteristics have a considerable influence on the elastic deformation of the bridge in the y direction.

Based on the above assumptions, Fig. 1 illustrates a simplified suspension electromagnet-bridge coupling model. Where y_B is the vertical displacement of the bridge, y_E is the vertical displacement of the electromagnet relative to the reference plane, and δ is the distance between the electromagnet and the bridge.

The vertical motion of the bridge can be formulated as:

Variables			
x	Axial coordinate of the bridge	N	Number of coils
T	Time	A	Electromagnet area
EI_B	Bending rigidity	μ_0	Magnetic permeability of the vacuum
ρ_B	Density of the bridge	u_0	Initial voltage
$f(x,t)$	Electromagnetic forces, which depend on the vehicle location	i_0	Initial current
λ_B	Spatial wavelength of the first mode	F_{E0}	Initial electromagnetic force
$F_{Ei}(t)$	Electromagnetic forces ($x=0.5L_B$)	k_p	Gap feedback coefficient
Ω	Spatial circular frequency of the guideway irregularity	k_d	Gap first feedback derivative
$S(\Omega)$	PSD ($mm^2 \cdot m$)	k_{ep}	Equivalent magnetic dynamic stiffness
A ~ G	Spectral characteristic parameters	k_{ed}	Equivalent magnetic dynamic damping
α^2	Interference intensity of the Gaussian white noise	ρ	Canonical transformation variate
β	center frequency	ξ_B	Damping ratio of the bridge
σ^2	Variance of the guideway irregularity, with $\xi(x)=R_\xi(0)$	ω_B	Self-frequency of the bridge
$S_\xi(\omega)$	Spectral density of the shaping filter	R	Resistance
m_E	Mass of the maglev vehicle	$-f_v$	Aerodynamic drop
m_B	Mass of the bridge	$\xi_1(t)$	Random irregularity
y_E	Vertical displacement of the electromagnets	$\sigma(H)$	Diffusion coefficient
y_B	Bridge vertical displacement	ρ	Canonical transformation variate
L_E	Magnet length	δ	Measurement gap between the electromagnet and bridge
$+f_v$	Aerodynamic lift	δ_0	Initial measurement gap
$B(t)$	Unit Wiener process	$H(t)$	Slowly varying stochastic process
$m(H)$	Drift coefficient	α_1	Canonical transformation variate

Table 1. Variables used in the model.

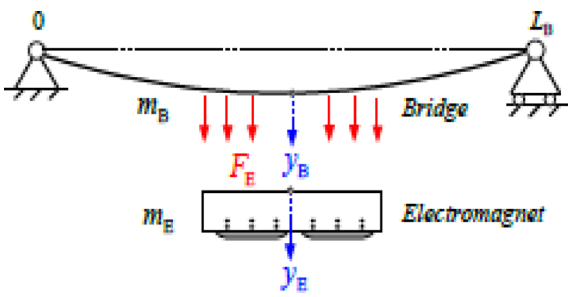

Figure 1. Minimal model.

$$EI_B \frac{\partial^4 y_B(x,t)}{\partial x^4} + \rho_B \frac{\partial^2 y_B(x,t)}{\partial t^2} = f(x,t) \tag{25}$$

where x is the transverse coordinate of the bridge, EI_B is the bending stiffness of the bridge, ρ_B is the linear density of the bridge, and $f(x,t)$ is the vertical force acting on the bridge.

$$\omega_B = \lambda_B^2 \sqrt{EI_B/\rho_B}$$

$$\phi_B(x) = sin(\lambda_B(x)) \tag{26}$$

When only the first mode is considered, $\lambda_B = \pi / L_B$. The solution to Eq. (1) can be expressed as,

$$y_B(x,t) = \phi_B(x) q_B(t) \ddot{q}_B(t) + 2\xi_B \omega_B \dot{q}_B(t) + \omega_B^2 q_B(t) = 2\rho_B^{-1} L_B^{-1} \sum_{i=1:N_E} \phi_B(x_i) F_{Ei}(t) \tag{27}$$

where q_B is the first-order generalized time domain coordinate of the bridge. By multiplying both sides of the above resultant equation by $\phi B(x)$ $\phi_{B(x)}$ and then integrating both sides from 0 to L_B we obtain:

$$y_B(x,t) = \phi_B(x) q_B(t) \tag{28}$$

The bridge's vertical displacement equation as

$$\ddot{y_B}(t) + 2\xi_B \omega_B \dot{y_B}(t) + \omega_B^2 y_B(t) = 2m_B^{-1} \phi_B^{-1} \sum_{i=:N_E} \phi_B(x_i) F_{Ei}(t) \tag{29}$$

Levitation model with feedback control. The electromagnetic forces can be simplified as long as the basic accuracy requirements are satisfied. Simplifications for the magnet-current relationship is linear near the ideal equilibrium point. The equivalent magnet dynamic stiffness and equivalent magnet dynamic damping are constant values [5]. The latter is related to the gap derivative. The equations of the electromagnetic forces as follows:

$$\begin{cases} F_{Ei} = F_{E0} + k_{ep}(\delta - \delta_0) + k_{ed}\,\dot{\delta} \\ F_{E0} = \dfrac{\mu_0 N^2 A}{4} \left(\dfrac{i_0}{\delta_0} \right)^2 \\ k_{ep} = \dfrac{a_1}{\delta_0^2} + \dfrac{a_2}{\delta_0^3} \\ k_{ed} = a_3 k_d \dfrac{u_0 + k_d\,\dot{\delta}}{\delta_0^2} \\ a_1 = \dfrac{\mu_0 N^2 A k_p}{2} (k_p \delta_0 - i_0 R) \\ a_2 = -\dfrac{\mu_0 N^2 A}{2} (k_p \delta_0 - i_0 R)^2 \\ a_3 = \dfrac{\mu_0 N^2 A}{2} \end{cases} \tag{30}$$

Guideway irregularity. The rail irregularity in a maglev line is the main source of extrinsic interference. At present, both the maglev lines in Shanghai[31] and the Korean Institute of Machinery and Materials [41] implement their own measuring methods and have collected corresponding data. Due to the guideway irregularity caused by concrete shrinkage, concrete creep and vehicle loads, the wavelength is considered equal to the span of the bridge and the frequency is related to the vehicle speed.

Bounded noise includes harmonic variations with a maximum amplitude, a constant frequency, and random phases [45–50]. It can be expressed via the stationary random process $\xi_1(t)$ as follows:

$$\xi_1(t) = A_v \cos(\Omega t + \sigma_1 B(t) + \Delta) \tag{31}$$

where Ω is a constant center frequency with $\Omega = \pi\ V/L$, with V being the vehicle speed and L being the bridge length, A_v is the maximum deflection of the bridge in the vertical direction, t is time, σ_1 is the strength of the frequency perturbations, $B(t)$ is a unit Wiener process, and Δ is a random phase that is uniformly distributed in $[0, 2\pi]$[37]. Its auto covariance functions are

$$\begin{cases} C_{\xi_1(t)}(\tau) = \dfrac{A_v^2}{2} \exp(-\dfrac{\sigma^2|\tau|}{2}) \cos\Omega\tau \\ C_{\dot{\xi}_1(t)}(\tau) = \dfrac{(A_v\Omega)^2}{2} \exp(-\dfrac{\sigma^2|\tau|}{2}) \cos\Omega\tau \end{cases} \tag{32}$$

and their corresponding spectral densities are

$$\begin{cases} S_{\xi}\omega = \dfrac{\sigma_1^2 A_v^2}{4\pi}\left[\dfrac{\omega^2+\Omega^2+\sigma_1^4/4}{(\omega^2-\Omega^2-\sigma_1^4/4)^2+\sigma_1^4\omega^2}\right] \\ S_{\dot{\xi}}\omega = \dfrac{\sigma_1^2 (A_v\Omega)^2}{4\pi}\left[\dfrac{\omega^2+\Omega^2+\sigma_1^4/4}{(\omega^2-\Omega^2-\sigma_1^4/4)^2+\sigma_1^4\omega^2}\right] \end{cases} \tag{33}$$

The variance of the bounded noise [43] is

$$\begin{cases} C_{\xi}(0) = \dfrac{A_v^2}{2} \\ C_{\dot{\xi}}(0) = \dfrac{(A_v\Omega)^2}{2} \end{cases} \tag{34}$$

A comparison between the filter, the experimental line, and the literature is shown in Fig. 2, where it is evident that there is numerical consistency.

Dynamic differential equations.

$$\begin{cases} m_B\ddot{y_B} = -2m_B\xi_B\omega_B(\dot{y_B}+\dot{\xi(t)}) - m_B\omega_B^2(y_B+\xi(t)) + \sigma[(F_{E0}+k_{ep}(y_E-y_B-\xi(t))+k_{ed}(\dot{y_E}-\dot{y_B}-\dot{\xi(t)})] \\ m_E\ddot{y_E} = -\sigma[f_{mo}+k_{ep}(y_E-y_B-\xi(t))+k_{ed}(\dot{y_E}-\dot{y_B}-\dot{\xi(t)})] \\ \sigma = 2\phi_B(x)\phi^{-1}(\pi x/L_B)\sum_{i=1}^{n}\int_{x_{LEi}}^{x_{LEi}+L_E}\phi_B^2(x)dx \end{cases} \tag{35}$$

In the above equations, σ is the amplification factor of multiple suspension units. Through simplification, the dynamic differential equations can be expressed as:

$$\begin{cases} \dot{q_1} = p_1 \\ \dot{p_1} = \beta_{10}p_1 + \beta_{11}(p_2-p_1) + \alpha_{10}q_1 + \alpha_{11}(q_2-q_1) + \gamma_{10} + E_{11}\xi_1(t) + E_{12}\xi_2(t) \\ \dot{q_2} = p_2 \\ \dot{p_2} = \beta_{20}p_2 + \beta_{21}(p_2-p_1) + \alpha_{20}q_2 + \alpha_{21}(q_2-q_1) + \gamma_{20} + E_{21}\xi_1(t) + E_{22}\xi_2(t) \end{cases} \tag{36}$$

where

$$\begin{cases} q_1 = y_B, q_2 = y_E, p_1 = y_B \\ \beta_{20} = 0, \beta_{21} \\ \xi_1(t) = \cos(\Omega t + \sigma_1 B(t) + \Delta), \xi_2(t) = sin(\Omega t + \sigma_2 B(t) + \Delta), \\ E_{11} = -\sigma k_{ep}A_v, E_{12} = -\sigma k_{ed}A_v\Omega, E_{21} = \sigma k_{ep}A_v, E_{22} = \sigma k_{ed}A_v\Omega, \end{cases}$$

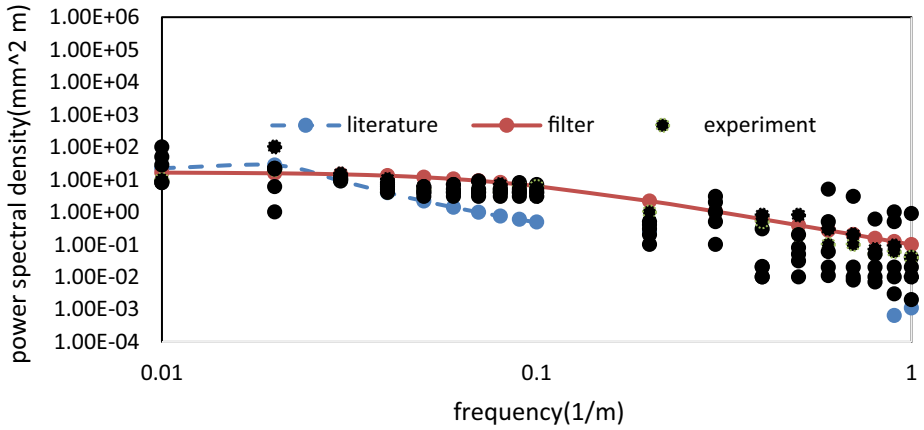

Figure 2. Comparison between the filter, the experiment line, and the literature reference.

Analysis of the Lyapunov exponent and stationary probability

To better evaluate the case study, the calculation process is elaborated further.

The differential equations for the motion integrals H_1 and H_2 and the angle variables θ_1 and θ_2 are expressed as follows:

$$\begin{cases} \frac{dH_1}{dt} = p_1[(\beta_{10}-\beta_{11})p_1 + E_{11}\xi_1(t) + E_{12}\xi_2(t)] \\ \frac{dH_2}{dt} = p_2[(\beta_{20}+\beta_{21})P_2 + E_{21}\xi_1(t) + E_{22}\xi_2(t)] \\ \frac{d\theta_1}{dt} = \omega_1 + \frac{\partial\theta_1}{\partial p_1}[(\beta_{10}-\beta_{11})P_1 + E_{11}\xi_1(t) + E_{12}\xi_2(t)] \\ \frac{d\theta_2}{dt} = \omega_2 + \frac{\partial\theta_2}{\partial p_2}[(\beta_{20}+\beta_{21})P_2 + E_{21}\xi_1(t) + E_{22}\xi_2(t)] \end{cases} \tag{37}$$

where

$$\begin{cases} H_1 = \frac{p_1^2}{2} - \omega_B^2 q_1^2/2 - \alpha_{11}(q_1 - q_2)^2/2 + \gamma_{10}q_1 \\ H_2 = \frac{p_2^2}{2} - \omega_E^2 q_2^2/2 + \alpha_{21}(q_1 - q_2)^2/2 + \gamma_{20}q_2 \end{cases}$$

Only external resonant vibration. Consider a system with external resonance but no internal resonance. Suppose that there is a single external resonant relation [36].

$$\Omega_1 - 2\omega_1 = \varepsilon\Theta \tag{38}$$

where ε and Θ can be regarded as small detuning parameters. The new variable ψ is introduced, as defined in Eq. (39).

$$\psi = \Omega_1 t + \sigma_1 B_1(t) + \Delta_1 - 2\theta_1 \tag{39}$$

The differential equations for H_1, H_2, and ψ, are stated below:

$$\begin{cases} dH_1 = [(\beta_{10}-\beta_{11})H_1 + \frac{E_{11}}{2\omega_1}sin\psi H_1 + \frac{E_{12}}{2\omega_1}cos\psi H_1)]dt \\ dH_2 = [(\beta_{20}+\beta_{21})H_2 + \frac{E_{21}}{2\omega_2}sin\psi H_2 + \frac{E_{22}}{2\omega_2}cos\psi H_2]dt \\ d\psi = [(\Omega_1 - 2\omega_1) + \frac{E_{11}}{2\omega_1}\cos\psi + \frac{E_{12}}{2\omega_1}sin\psi]dt + \sigma_1 dB_1(t) \end{cases} \tag{40}$$

The differential equations for ρ and α_1 can be formulated as follows

$$\begin{cases} d\rho = \frac{1}{2}(\beta_{20}+\beta_{21} + (-\beta_{20}-\beta_{21} - \frac{E_{21}}{2\omega_2}\sin\psi - \frac{E_{22}}{2\omega_2}\cos\psi + \beta_{10} - \beta_{11} + (\frac{E_{11}}{2\omega_1}\sin\psi + \frac{E_{21}}{2\omega_1}\cos\psi))\alpha_1 \\ \quad + \sqrt{\alpha_1(1-\alpha_1)} + (\frac{\alpha_{11}}{\omega_2} - \frac{\alpha_{21}}{\omega_1})sin\varphi)dt \\ d\alpha_1 = (-\beta_{20}-\beta_{21} - \frac{E_{21}}{2\omega_2}\sin\psi - \frac{E_{22}}{2\omega_2}\cos\psi + \beta_{10} - \beta_{11} + (\frac{E_{11}}{2\omega_1}\sin\psi + \frac{E_{21}}{2\omega_1}\cos\psi))\alpha_1(1-\alpha_1)dt \end{cases} \tag{41}$$

The averaging FPK equation presented by Zhu (2002) [17] that is associated with ψ is

$$\sigma_1^2\frac{d^2p}{d\psi^2} - 2\frac{d}{d\psi}[((\Omega_1 - 2\omega_1) + (\frac{E_{11}}{2\omega_1}cos(\psi) + \frac{E_{12}}{2\omega_1}sin(\psi))p] = 0 \tag{42}$$

The solution that satisfies the periodic condition is

$$\begin{aligned} p(\psi) = C\exp\{\frac{2}{\sigma_1^2}[(\Omega_1 - \omega_1)\psi + \frac{E_{11}}{2\omega_1}sin(\psi) + \frac{E_{12}}{2\omega_1}cos(\psi)]\} \\ \int_{\psi}^{2\pi+\psi}\exp\{-\frac{2}{\sigma_1^2}\times[(\Omega_1-\omega_1)\psi + \frac{E_{11}}{2\omega_1}sin(\psi) + \frac{E_{12}}{2\omega_1}cos(\psi)]d\psi \end{aligned} \tag{43}$$

where C is a normalized constant. The mean $d\alpha_1$ can be calculated as:

$$d\alpha_1 = (-\beta_{20}-\beta_{21}-\frac{E_{21}}{2\omega_2}\sin\psi-\frac{E_{22}}{2\omega_2}\cos\psi+\beta_{10}-\beta_{11}+(\frac{E_{11}}{2\omega_1}\sin\psi+\frac{E_{21}}{2\omega_1}\cos\psi))\alpha_1(1-\alpha_1)dt = A(\alpha)dt \tag{44}$$

If $A(\alpha) > 0, \alpha_1 \to 1$ and $p(\alpha_1, \psi) = p(\psi)\delta(1)$. if $A(\alpha) < 0, \alpha_1 \to 0$ and $p(\alpha_1, \psi) = p(\psi)\delta(0)$
The equation can be expressed as:

$$\lambda_1 = \int_0^{2\pi}\int_0^1 \frac{1}{2}A(\alpha)p(\alpha_1, \psi)d\alpha_1 d\psi \tag{45}$$

Some results we obtained via simulations. The joint probability density $p(\alpha_{1,}\psi)$ represents the centralized peak when $\Psi=0$ and $\alpha_1=0$. In Fig. 3, when $\psi=0$ and $\alpha_1 = 0.5$, the stationary joint probability density $p(\alpha_{1,}\psi)$ shows a peak. In Fig. 3, when $\Omega_1-2\omega_1 = 0$, the first time of resonating to exceed is the shortest. As shown in Fig. 3 and Fig. 4, the cross-stable region in the frequency-excitation amplitude plane has a valley shape when $\lambda_1 = 0$. As the guideway irregularity coefficient E_{11} increases, the maximum Lyapunov exponents increase gradually from their initial small stable state, as shown in Fig. 5. A comparison between the stochastic averaging method and the numerical simulation is also shown in Fig. 5, where the numerical consistency between the results is evident. The random average method is more vivid from the grasp of the critical value of total energy and the changing trend. Through the grasp of displacement, the numerical simulation has a large amount of calculation.

Both internal and extrinsic resonance. Consider a case with primary external resonance between the first bounded noise excitation and the first oscillator. The primary internal resonance between the two oscillators [36] can be expressed as:

$$\begin{cases}\Omega_1-2\omega_1 = \varepsilon\Theta\\ \omega_2-\omega_1 = \varepsilon\eta\end{cases} \tag{46}$$

where Θ and η are detuning parameters [26]. The new variables ψ and Φ are introduced as angle differences.

$$\begin{cases}\psi = \Omega_1 t + \sigma_1 B_1(t) + \Delta_1-2\theta_1\\ \Phi = \theta_2-\theta_1\end{cases} \tag{47}$$

The differential equations for H_1, H_2, ψ, and Φ can be formulated as

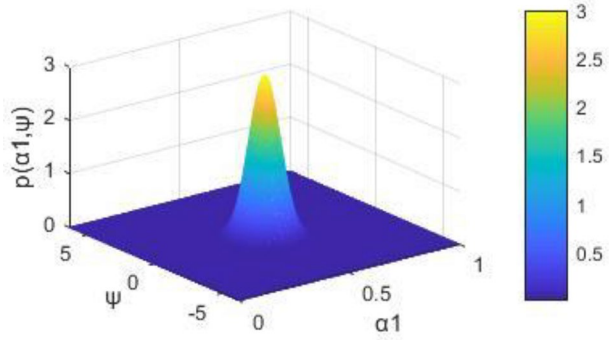

Figure 3. Stationary probability densities in a system with external excitation only.

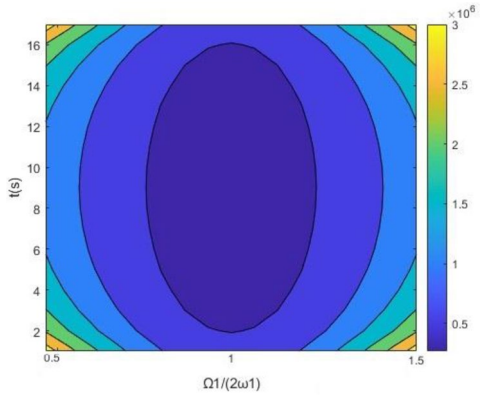

Figure 4. Time–frequency-amplitude region of cross stability in a system with external excitation only.

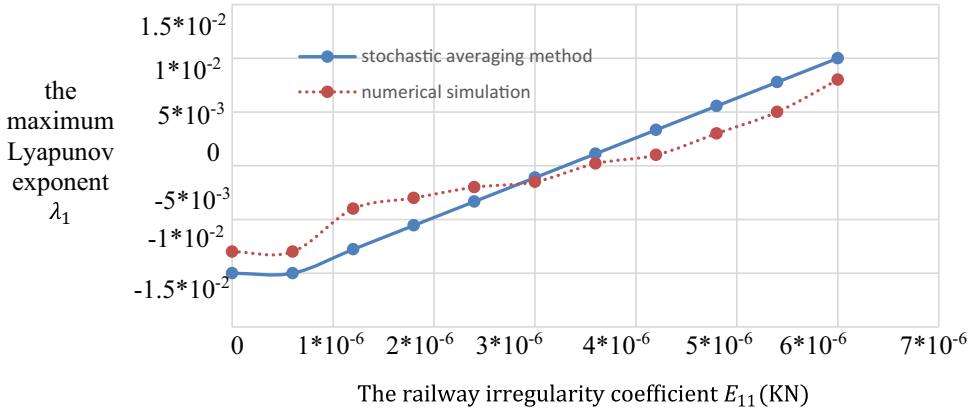

Figure 5. Lyapunov exponent in a system with external excitation only.

$$\begin{cases} dH_1 = [(\beta_{10} - \beta_{11})H_1 + \dfrac{E_{11}}{2\omega_1} sin\psi H_1 + \dfrac{E_{12}}{2\omega_1} cos\psi H_1 + \dfrac{\alpha_{11}\sqrt{H_1 H_2}}{\omega_2} sin\phi)]dt \\ dH_2 = [(\beta_{20} + \beta_{21})H_2 + \dfrac{E_{21}}{2\omega_2} sin\psi H_2 + \dfrac{E_{22}}{2\omega_2} cos\psi H_2 - \dfrac{\alpha_{21}\sqrt{H_1 H_2}}{\omega_1} sin\phi]dt \\ d\psi = [(\Omega_1 - 2\omega_1) + \dfrac{E_{11}}{2\omega_1}\cos\psi + \dfrac{E_{12}}{2\omega_1} sin\psi + \dfrac{\alpha_{11}}{\omega_2}\sqrt{\dfrac{H_2}{H_1}}\cos\phi]dt + \sigma_1 dB_1(t) \\ d\phi = [(\omega_2 - \omega_1) + \dfrac{E_{11}}{4\omega_1}\cos\psi + \dfrac{E_{12}}{4\omega_1} sin\psi + \dfrac{\alpha_{11}}{\omega_2}\sqrt{\dfrac{H_2}{H_1}}\cos\phi - \dfrac{\alpha_{21}}{\omega_1}\sqrt{\dfrac{H_1}{H_2}}\cos\phi]dt \end{cases} \tag{48}$$

The differential equations for ρ and α_1 can be formulated as

$$\begin{cases} d\rho = \dfrac{1}{2}(\beta_{11} + \beta_{21} + (\beta_{20} + \beta_{10} - \beta_{11} - \beta_{21} + \dfrac{E_{11}}{2\omega_1}\sin\psi + \dfrac{E_{12}}{2\omega_1}\cos\psi - \dfrac{E_{21}}{2\omega_2}\sin\psi - \dfrac{E_{22}}{2\omega_2}\cos\psi)\alpha_1 \\ \quad + (\dfrac{\alpha_{11}}{\omega_2} - \dfrac{\alpha_{21}}{\omega_2})\sin\Phi\sqrt{\alpha_1(1-\alpha_1)})dt \\ d\alpha_1 = \beta_{20} + \beta_{10} - \beta_{11} - \beta_{21} + \dfrac{E_{11}}{2\omega_1}\sin\psi + \dfrac{E_{12}}{2\omega_1}\cos\psi - \dfrac{E_{21}}{2\omega_2}\sin\psi - \dfrac{E_{22}}{2\omega_2}\cos\psi)\alpha_1(1-\alpha_1) + (\sqrt{\alpha_1(1-\alpha_1)} \\ \quad (1-\alpha_1)\dfrac{\alpha_{11}}{\omega_2}\sin\Phi - \sqrt{\alpha_1(1-\alpha_1)}\alpha_1\dfrac{\alpha_{21}}{\omega_2}\sin\Phi)dt \end{cases} \tag{49}$$

$p(\alpha_1, \psi, \Phi)$ can be derived from the following equation, the derivation of which can be found in [17].

$$\frac{\partial p}{\partial t} = \frac{\partial m_1}{\partial \alpha_1} + \frac{\partial G}{\partial \psi} + \frac{\partial K}{\partial \Phi} + \frac{\sigma_1^2}{2}\frac{\partial p^2}{\partial \psi^2} \tag{50}$$

The transition probability density is obtained from the solution of the FPK equation:$p = p(\alpha_1, \psi, \Phi, t|\alpha_0, \psi_0, \Phi_0)$.

The maximum Lyapunov exponent can be expressed as:

$$\lambda_1 = \int_0^1\int_0^{2\pi}\int_0^{2\pi} \frac{1}{2}(\beta_{11} + \beta_{21} + (\beta_{20} + \beta_{10} - \beta_{11} - \beta_{21} + \frac{E_{11}}{2\omega_1}\sin\psi + \frac{E_{12}}{2\omega_1}\cos\psi - \frac{E_{21}}{2\omega_2}\sin\psi - \frac{E_{22}}{2\omega_2}\cos\psi)\alpha_1 + (\frac{\alpha_{11}}{\omega_2} - \frac{\alpha_{21}}{\omega_2})\sin\Phi\sqrt{\alpha_1(1-\alpha_1)})]p(\alpha_1, \psi, \phi)d\alpha_1 d\psi d\phi \tag{51}$$

A numerical calculation is helpful for determining reason for this resonance. In Fig. 6, when $\psi = 0$, $\Phi = 0$, the stationary joint probability density $p(\Phi, \psi)$ shows a peak. The joint probability density $p(\Phi, \psi)$ represents a centralized distribution with the angle differences $\Psi = 0$ and $\Phi = 0$. Figures 6 and 7 show the stable and unstable regions in the frequency-excitation amplitude plane, which is resembles a saddle shape. As the guideway irregularity coefficient E_{11} increases, the maximum Lyapunov exponents start from their initial small stable state and rise in a step-wise manner, as shown in Fig. 8. A comparison between the stochastic averaging method and the numerical simulation is also shown in Fig. 8, where numerical consistency between the stochastic averaging method and the numerical simulation is also shown in Fig. 8, where numerical consistency can be observed. The random average method is more vivid from the grasp of the critical value of total energy and the changing trend. Through the grasp of displacement, the numerical simulation has a large amount of calculation.

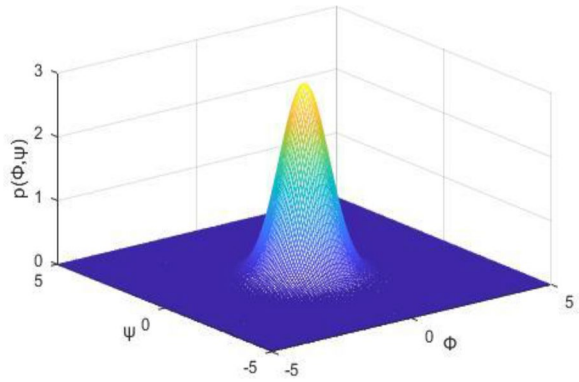

Figure 6. Stationary probability density of a system with both internal and external excitation.

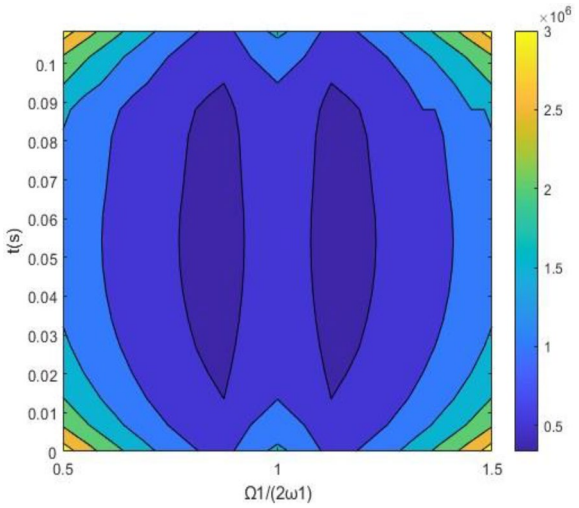

Figure 7. Time–frequency amplitude stable region in a system with both internal and external excitation.

Summary

In this paper, stochastic averaging method for a quasi-integrable Hamiltonian system under bounded noise is proposed in this paper. The forms and dimensions of the averaging equations depend on the number of internal and external resonant relations in the system. The proposed procedures were applied in the prediction of a high-speed maglev train-bridge coupled system responses under bounded noise. The results obtained from the reduced averaging FPK equation by using the finite difference and the successive over-relaxation iterative methods are consistent with simulations of the original system. It is noted that the proposed procedure may also be applicable in studying the reliability and stochastic stability of these systems under bounded noise. The results conclusively show that

- The joint probability density of different phases has a peak when the phases are close to each other.
- The stable region shrinks when the two resonance conditions are satisfied.
- When the unstable region in the phase diagram (E_{11}, $\Omega_j 2\omega_1$) is affected by only one external resonance, the external resonance reduces the stable region. The closer the external resonance frequency is to the system frequency, the smaller the size of the stable region. Moreover, as E_{11} increases, the maximum Lyapunov exponent changes from negative to positive, and the system shifts from stability to instability in a nearly linear manner.
- When the unstable region in the phase diagram (E_{11}, $\Omega_j 2\omega_1$) is affected by both internal and external resonance, the stable region shrinks as the energy is transferred from the first oscillator to the second oscillator during the two resonances. As E_{11} increases, the maximum Lyapunov exponent changes from negative to positive, and the system shifts from stability to instability in a step-wise manner.

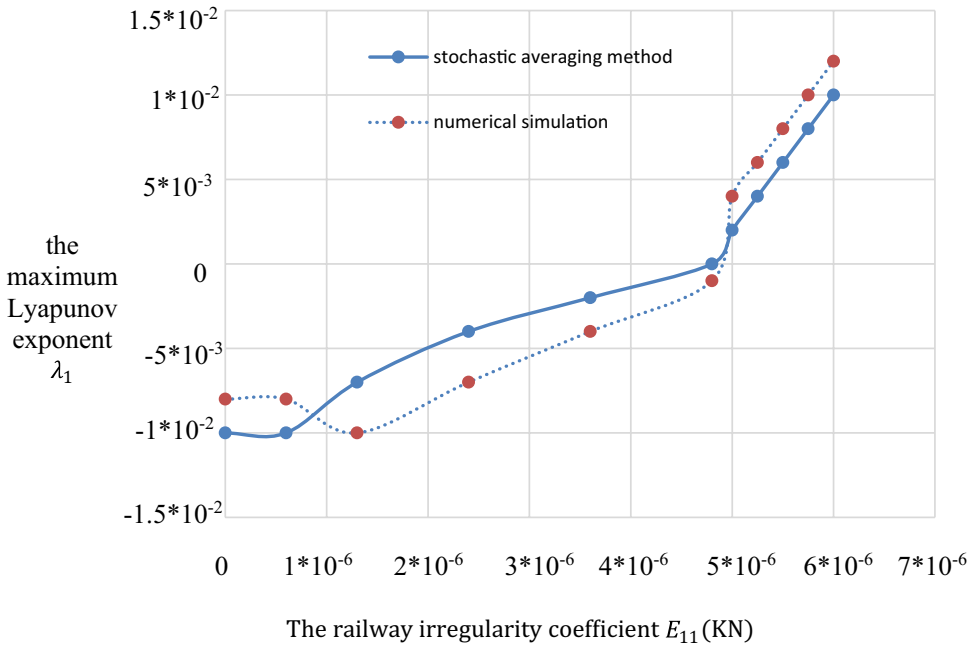

Figure 8. Lyapunov exponents of a system with both internal and external excitation.

Data availability

The data used in this study can be obtained from the corresponding author upon request.

Received: 19 December 2022; Accepted: 8 April 2023
Published online: 09 May 2023

References

1. Ahmed, R., Jun, Y. L., Azhar, M. F. & Junejo, N. U. R. Comprehensive study and review on maglev train system. *Appl. Mech. Mater.* **615**, 347–351 (2014).
2. Zhiyun, S. Dynamic interaction of high speed maglev train on girders and its comparison with the case in ordinary high speed railways. *J. Traffic Transp. Eng.* **1**(1), 1–6 (2001).
3. Wanming, Z., Chunfa, Z. & Chengbiao, C. On the comparison of dynamic effects on bridges of maglev trains with high-speed wheel/rail trains. *J. Traffic Transp. Eng.* **1**(1), 7–12 (2001).
4. Wanming, Z. & Chunfa, Z. Dynamics of maglev vehicle/guideway systems (I) magnet/rail interaction and system stability. *Chin. J. Mech. Eng.* **41**(7), 1–10 (2005).
5. Chunfa, Z. & Wanming, Z. Dynamics of maglev vehicle/guideway systems (II) modeling and simulation. *Chin. J. Mech. Eng.* **41**(8), 163–175 (2005).
6. Li, J. *et al.* The modeling and analysis for the self-excited vibration of the maglev vehicle-bridge interaction system. *Math. Probl. Eng.* **709583**, 1–10 (2015).
7. Mingwei, P. *et al.* Discussion on high-speed maglev vehicle's coupling mechanism between vehicle and bridge. *Railway Locomotive & Car.* **5**, 9–13 (2007).
8. Jinhui, Li. *et al.* Self-excited vibration problems of maglev vehicle-bridge interaction system. *J. Central South Univ.* **21**(11), 4184–4192 (2014).
9. Jinhui, L., Jie, L. & Danfeng, Z. The active control of maglev stationary self-excited vibration with a virtual energy harvester. *IEEE Trans. Industr. Electron.* **62**(5), 2942–2951 (2015).
10. Jinhui, L. *et al.* A practical control strategy for the maglev self-excited resonance suppression. *Math. Probl. Eng* **8071938**, 1–9 (2016).
11. Fryba, L. A rough assessment of railway bridges for high speed trains. *Eng. Struct.* **23**, 548–556 (2001).
12. Yau, J. D. & Yang, Y. B. Vertical accelerations of simple beams due to successive loads traveling at resonant speeds. *J. Sound Vib.* **289**(1), 210–228 (2006).
13. Kwark, J.W., *et a1*. Dynamic behavior of two-span continuous concrete bridges under moving high-speed train. *Computers & Structures.* **82**(4–5), 463–474(2004).
14. He, Xia. *et al.* Vibration resonance and cancellation of simply supported bridges under moving train loads. *J. Eng. Mech.* **140**(5), 4014015 (2014).
15. Yang, Y. B., Yau, J. D. & Wu, Y.S. *Vehicle-bridge interaction dynamics: with applications to high-speed railways* (World Scientific, 2004).
16. Sun, Y. *et al.* Hopf bifurcation analysis of maglev vehicle–guideway interaction vibration system and stability control based on fuzzy adaptive theory. *Comput. Ind.* **108**, 197–209 (2019).
17. Lanzara, E., Mantegna, R.N., Spagnolo, B. & Zangara, R. Experimental study of a nonlinear system in the presence of noise: the stochastic resonance. *Am. J. Phys.* **65**, 341–349 (1997).
18. Mikhaylov, A.N. *et al.* Stochastic resonance in a metal-oxide memristive device. *Chao Solitons Fractals* **144**, 110723 (2021).

19. Fiasconaro, A., Mazo, J. J. & Spagnolo, B. Noise-induced enhancement of stability in a metastable system with damping. *Phys. Rev. E* **82**, 041120 (2010).
20. Filatov, D.O. *et al.* Noise-induced resistive switching in a memristor based on ZrO2(Y) /Ta2O5 stack. *J. Stat. Mech. Theory Exp.* **2019**, 124026 (2019).
21. Chertkov, M., Chernyak, V. & Maximov, Y. Gauges, loops, and polynomials for partition functions of graphical models. *J. Stat. Mech. Theory Exp.* **2020**, 124006 (2020).
22. Agudov, N.V. *et al.* Nonstationary distributions and relaxation times in a stochastic model of memristor. *J. Stat. Mech. Theory Exp.* **2020**, 024003 (2020).
23. Carollo, A., Valenti, D. & Spagnolo, B. Geometry of quantum phase transitions. *Phys. Rep.* **838**, 1–72 (2020).
24. Carollo, A. *et al.* On quantumness in multi-parameter quantum estimation. *J. Stat. Mech. Theory Exp.* **2019**, 094010 (2019).
25. Ushakov, Y. V., Dubkov, A. A. & Spagnolo, B. Spike train for consonant and dissonant musical accords in a simple auditory sensory model. *Phys Rev E* **81**, 041911 (2010).
26. Yakimov, A. V. *et al.* Measurement of the activation energies of oxygen ion diffusion in yttria stabilized zirconia by flicker noise spectroscopy. *Appl. Phys. Lett.* **114**(25), 253506–253511 (2019).
27. Huang, Z. L. & Zhu, W. Q. Stochastic averaging of strongly non-linear oscillators under bounded noise excitation. *J. Sound Vib.* **254**(2), 245–267 (2002).
28. Zhu, W. Q., Huang, Z. L., Ko, J. M. & Ni, Y. Q. Optimal feedback control of strongly non-linear systems excited by bounded noise. *J. Sound Vib.* **274**, 701–724 (2004).
29. Zeshen, C. & Chengguo, W. Covariance analysis method for vehicle random vibration. *China Railway Sci.* **22**(4), 1–8 (2001).
30. Jin, Z., Qiang, S. & Li, X. Uniform white noise model for time-delay multi-dimensional rail irregularity excitation. *J. Southwest Jiaotong Univ.* **42**(3), 269–273 (2007).
31. Shi, J. *et al.* Measurements and analysis of track irregularities on high speed maglev lines. *J. Zhejiang Univ. Sci. A* **15**(6), 385–394 (2014).
32. Dimentberg, M. Stability and subcritical dynamics of structures with spatially disordered travelling parametric excitation. *Probab. Engrg. Mech.* **7**, 131–134 (1991).
33. Lin, Y. K., Li, Q. C. & Su, T. C. Application of a new turbulence model in predicting motion stability of wing-excited long-span bridge. *J. Wind Engrg. Ind. Aerodyn.* **49**, 507–516 (1993).
34. Deng, J., Zhong, Z. & Liu, A. Stochastic stability of viscoelastic plates under bounded noise excitation. *Eur. J. Mech. A Solids* **78**, 103849 (2019).
35. Lyon, R. H., Heckl, M. & Hazelgrove, C. B. Response of hard-spring oscillator to narrow-band excitation. *J. Acoust. Soc. Am.* **33**, 1404–1411 (1961).
36. Stratonovich, R. L. *Topics in the theory of Random Noise* 1 (Gordon and Breach, New York, 1967).
37. Huang, Z. L. & Zhu, W. Q. Stochastic averaging of quasi-integrable Hamiltonian systems under bounded noise excitations. *Probab. Eng. Mech.* **19**(3), 219–228 (2004).
38. Liu, W. Y., Zhu, W. Q. & Huang, Z. L. Effect of bounded noise on chaotic motion of duffing oscillator under parametric excitation. *Chaos Solitons Fractals* **12**, 527–537 (2001).
39. Zhang, Bo., Zeng, J. & Liu, W. Research on stochastic stability and stochastic bifurcation of suspended wheelset. *J. Mech. Sci. Technol.* **29**(8), 3097–3107 (2015).
40. Wang, L. C., Li, J. H., Zhou, D. F. & Li, J. An experimental validated control strategy of maglev vehicle-bridge self-excited vibration. *Appl. Sci.* **7**, 38 (2017).
41. Yu, H. & Wu, D. Structure and dynamics of maglev system guideway. *China Metros* **9**, 38–40 (2006).
42. Xu, W., Li, W. & Zhao, J. F. Stochastic stabilization of uncontrolled and controlled Duffing-vander Pol systems under Gaussian white-noise excitation. *J. Sound Vib.* **290**(3), 723–735 (2006).
43. Wang, D. *et al.* Dynamic interaction of the low-to-medium speed maglev train and bridges with different deflection ratios: experimental and numerical analyses. *Adv. Struct. Eng.* **23**(10), 2239–2413 (2020).
44. Ming, Xu., Jin, X., Wang, Y. & Huang, Z. Optimal bounded control for maximizing reliability of Duhem hysteretic systems. *Appl. Math. Mech.* **36**(10), 1337–1346 (2015).
45. Xiong, J.-J. A nonlinear fracture differential kinetic model to depict chaotic atom motions at a fatigue crack tip based on the differentiable manifold methodology. *Chaos Solitons Fractals* **5**(29), 1240–1255 (2006).
46. Charikleia, D. S. & Dimitrakopoulos, E. G. A modified bridge system method to characterize decouple vehicle-bridge interaction. *Acta Mech.* **231**(9), 3825–3845 (2020).
47. Zhou, D., Li, J. & Hnsen, C. H. Suppression of the stationary maglev vehicle-bridge coupled resonance using a tuned mass damper. *J. Vib. Control* **19**(2), 191–203 (2013).
48. Wang, L., Li, J., Zhou, D., & Li, J. The underlying principles of self-excited vibration in maglev vehicle-bridge coupled system. In *2016 Chinese Control and Decision Conference (CCDC)*, Yinchuan, China, pp 4119–4124.
49. Zhu, W. Q. & Liu, Z. H. Homoclinic bifurcation and chaos in coupled simple pendulum and harmonic oscillator under bounded noise excitation. *Int. J. Bifurc. Chaos* **15**(1), 233–243 (2011).
50. Li, J., Wei, X., Yang, X. & Sun, Z. Chaotic motion of Van der Pol-Mathieu-Duffing system under bounded noise parametric excitation. *J. Sound Vib.* **309**(1), 330–337 (2008).

Acknowledgements

The work was supported by the National Natural Science Foundation (Grant Number 51578549, 51708558, 52078485), the National Joint Natural Science Foundation (Grant Number U1934217), and the Fundamental Research Funds for the Central Universities of the Central South University (Grant Number 2016zzts079).

Author contributions

Y.L. contributed to the conception of the study, performed the data analyses and wrote the manuscript. Z.Y. and L.X. contributed significantly to analysis and manuscript preparation and helped perform the analysis with constructive discussions.

Competing interests

The authors declare no competing interests.

Additional information

Correspondence and requests for materials should be addressed to Y.L.

Reprints and permissions information is available at www.nature.com/reprints.

Publisher's note Springer Nature remains neutral with regard to jurisdictional claims in published maps and institutional affiliations.

Open Access This article is licensed under a Creative Commons Attribution 4.0 International License, which permits use, sharing, adaptation, distribution and reproduction in any medium or format, as long as you give appropriate credit to the original author(s) and the source, provide a link to the Creative Commons licence, and indicate if changes were made. The images or other third party material in this article are included in the article's Creative Commons licence, unless indicated otherwise in a credit line to the material. If material is not included in the article's Creative Commons licence and your intended use is not permitted by statutory regulation or exceeds the permitted use, you will need to obtain permission directly from the copyright holder. To view a copy of this licence, visit http://creativecommons.org/licenses/by/4.0/.

© The Author(s) 2023